Transport of citrate and polymer coated gold nanoparticles (AuNPs) in porous media: Effect of surface property and Darcy velocity

Wen, Chunyu; Broholm, Mette Martina; Dong, Jun; Uthuppu, Basil; Jakobsen, Mogens Havsteen; Fjordbøge, Annika Sidelmann

Published in:
Journal of Environmental Sciences

Link to article, DOI:
10.1016/j.jes.2020.02.026

Publication date:
2020

Document Version
Peer reviewed version

This is a post-peer-review, pre-copyedit version of an article published in Journal of Environmental Sciences. The final authenticated version is available online at:
https://doi.org/10.1016/j.jes.2020.02.026.

Transport of citrate and polymer coated gold nanoparticles (AuNPs) in porous media: effect of surface property and Darcy velocity

Chunyu Wen[1,2], Mette M. Broholm[1], Jun Dong[2], Basil Uthuppu[3], Mogens Havsteen Jakobsen[3], Annika S. Fjordbøge[1,*]

1. Department of Environmental Engineering, Technical University of Denmark, Kgs. Lyngby DK-2800, Denmark.
2. Key Lab of Groundwater Resources and Environment Ministry of Education, Jilin University, Changchun, 130021. China
3. Department of Micro- and Nanotechnology, Technical University of Denmark, Kgs. Lyngby DK-2800, Denmark

Abstract: With the release of nanoparticles (NPs) into the subsurface, it is imperative to better understand the fate and transport of NPs in porous media. Three types of stable AuNPs were used as model NPs to investigate the impact of surface coatings (type and coverage) and water velocity on the NP transport in a porous media (column studies). The NPs were electrostatic stabilized citrate AuNPs and sterically stabilized AuNPs with amphiphilic block co-polymer (PVA-COOH) in two particle/polymer ratios (weak vs. strong stabilization). The citrate AuNPs transport was sensitive to ionic changes in the mixing front of the plume, where destabilization occurred, and will therefore depend on the size/type of release. Blocking of deposition sites by aggregates was seen to facilitate transport, whereby a higher flow velocity (larger shadow zone) also resulted in better transport. The polymeric surface coating had great impact with steric repulsion as a main force contributing to the transport of NPs in the porous media. Sufficient polymer coating was crucial to obtain highly unfavorable attachment conditions (very low α) where the enhanced NP mobility was independent of the water velocity (comparable to solute tracer). Without sufficient steric stabilization, the transport and recovery was significantly reduced compared to the solute tracer, but increased with increasing water velocity. This highlights the importance of sufficient surface coating to achieve enhanced mobility, but also the increased risk of spreading to down-gradient receptors. For the (weakly) sterically stabilized NPs, the loss of polymer through ligand exchange with the porous media negates transport.

Keywords:
Gold nanoparticles
Transport
Flow velocity
Stabilization
Ligand exchange
Blocking

---

* Corresponding author. E-mail: asfj@env.dtu.dk (Annika S. Fjordbøge)

Introduction

The use of engineered nanoparticles (ENPs) in electronic, biomedical, personal care products and environmental remediation has emerged and expanded rapidly in recent years (Daniel and Astruc, 2004; He et al., 2009; Panyala et al., 2009). Due to their unique size-dependent physical and chemical properties, their potential risks and impacts to the environment, in particular, environmental application such as *in situ* remediation of contaminants, is of concern (Dong et al., 2013; Grieger et al., 2010). NPs of interest for *in situ* remediation include metal or metal oxide NPs, and carbon nanotubes (Wang et al., 2014, 2016; Yang et al., 2015).

Bare NPs, due to their high surface energy, tend to aggregate in suspension and attach to solid phase media, thereby exhibiting poor performance in application (Hotze et al., 2010; O'Carroll et al., 2013; Phenrat et al., 2008). Improvement of ENPs performance (stability, specific targeting property and thereby likely mobility) may be realized through surface modification with polymers, polyelectrolytes or surfactants (Liu et al., 2016; Saleh et al., 2007; Zhao et al., 2016). The modification agents are attached to the NPs surfaces to create or enhance repulsive forces including osmotic repulsion, electrostatic double layer repulsion and electrosteric repulsion to counter van der Waals and any magnetic attraction forces, and thereby affect their behavior in suspension and their environmental fate (Godinez and Darnault, 2011; Sangani et al., 2019).

The risks related to ENPs in the subsurface as well as the effectiveness of *in situ* remediation at contaminated sites is based on the behavior of the NPs in the aquifers, whereby it is essential to obtain a better understanding of the fate and transport of NPs in water saturated porous media. Generally, due to particle-particle interaction (aggregation) and particle-collector interaction (deposition), some

of the released NPs are removed from the groundwater and deposited on the porous media (Bayat et al., 2015; Louie et al., 2016). Transport and deposition of NPs in saturated porous media is found to be highly variable and strongly dependent on the properties of the NPs (e.g. size, concentration, shape, surface charge and modification), the porous media (e.g. type, grain size and heterogeneity) and the geochemical conditions (e.g. pH, ion strength and natural organic matter) (El Badawy et al., 2013; Chan and Vikesland, 2014; Godinez and Darnault, 2011; He et al., 2009; Phenrat et al., 2008; Rahman et al., 2013; Tian et al., 2012). Moreover, the mobility of ENPs is also controlled by the groundwater velocity and/or the injection velocity. Ben-Moshe et al. (2010) reported that lower flow rates led to reduced mobility and stronger retention of NPs in the porous media, which is interpreted by the larger time-scale of attachment compared with the time-scale of NPs transport to the collector. Flow rates have also been found to affect the retention of TiO_2 in porous media by controlling the resident time, which is a key parameter. As the flow rate increases, the number of sites for attachment accessible to NPs are reduced (Toloni et al., 2016).

Tracking of NPs in porous media is challenging partly due to the difficulties in measuring ENPs in complex environmental samples with natural background colloids, dissolved species and ongoing transformation processes (Montaño et al., 2014). Colloidal gold nanoparticles (AuNPs) feature a wide range of potential applications due to the low toxicity, size and shape dependent plasmonic properties, well-established relatively easy functionalization and detectability at low concentrations. Due to these properties, Fjordbøge et al. (2019) proposed that colloidal AuNPs can be used as a potential model NP for studying the fate in porous media. The study found that the stability and mobility of post-grafted AuNPs under environmental relevant physicochemical conditions was highly dependent on the applied type of polymeric stabilizing agent (two types applied), while electrostatically stabilized citrate AuNPs were unstable and immobile. PVA-COOH stabilized AuNPs were found to be the most affected by the physicochemical conditions (of the polymeric stabilizers), but also the most mobile particles when good stability was obtained. Cirtiu et al. (2011) found that pre-grafting of NPs with polymers containing carboxylate binding groups (similar to PVA-COOH) resulted in smaller particles and better stability than post-grafting. Better stability and mobility of the PVA-COOH AuNPs may thereby be obtained by using pre-grafting in the synthesis process instead of post-grafting. The mobility was also found to be dependent on the size of the injected pulse of AuNPs, where a short duration pulse (0.2 PV) at a relatively high Darcy velocity (>3 m day^{-1}) was mainly investigated.

The behavior related to different types and particle coverages of stabilizing agents at other Darcy velocities, especially lower ones better resembling groundwater velocities, as well as the AuNP

transformation processes during transport in the porous media is also of interest. The scope of this paper is therefore to investigate the fate and transport of electrostatically stabilized (citrate) and sterically stabilized (amphiphilic block co-polymer) NPs at various flow velocities using AuNPs as model particles. Column experiments were conducted with citrate stabilized AuNPs and pre-grafted amphiphilic block co-polymer stabilized AuNPs in two particle/polymer concentration ratios (i.e. 1:0.5 and 1:10 (w/w)) to represent both partial and full NP surface coverage i.e. weak and strong steric stabilization. In order to observe the plateau behavior of the breakthrough curve an injection pulse of one PV was applied. The investigation of transformation processes during transport in the porous media was supported by measurements of UV-Vis spectra and AuNPs sizes in the effluent samples at different times. The combination of various surface properties and Darcy velocities may advance the current understanding of factors that govern the mobility of NPs in natural and engineered environmental systems.

1 Materials and Methods

1.1 Chemicals

Gold(III) chloride hydrate, sodium citrate dehydrate, and potassium bromide (KBr) were analytical pure (Sigma-Aldrich Corporation, St. Louis, MO, USA). The nontoxic, anionic triblock copolymer carboxylic-functionalized poly vinyl alcohol containing 1.0 mol% carboxylic acid units (PVA-COOH) was kindly provided by Kuraray Europe Nordic AB OY (Poval KM-118, viscosity 26.0–34.0 mPa s, degree of hydrolysis 95.5–98.5%). Deionized (DI) water was obtained from a 18.2 MΩ cm^{-1} LabostarTM 1-DI (Evoqua Water Technologies LLC, Germany) ultra-pure water system.

1.2 Synthesis of nanoparticles

The stock suspensions of AuNP were synthesized by the sodium citrate reduction method (Li et al., 2011). Forty-five mL DI water with controlled amounts of PVA-COOH (0, 15 and 300 mg for citrate, AuNPs:PVA-COOH (1:0.5) and AuNPs:PVA-COOH (1:10), respectively) was prepared in a 250 mL triple-neck round bottom flask fitted with a water condenser. The solution was stirred and kept in an oil bath at 70°C until PVA-COOH had dissolved. Twenty mL of 8.83 mmol L^{-1} gold(III) chloride solution ($HAuCl_4$) was added and the solution heated to 130°C. While the solution was boiling, additional 5 mL of 136 mmol L^{-1} sodium citrate dihydrate was added. The reaction was run until the suspension reached a wine red color. The suspension was boiled for additional 15 min and then cooled

to room temperature. The synthesized AuNPs stock suspension was used as is, without removing excess citrate, polymer or unreacted starting material. It is expected that free dissolved citrate will be present in the stock suspension, while the excess of polymer in the stock is expected to be minimal due to the strong affinity of the hydrophilic block towards the metal center. For especially the 1:10 particle/polymer ratio excess polymer in solution cannot be ruled out.

1.3 Column experiments

Column experiments were conducted in transparent polyvinyl chloride columns (30 cm long, inner diameter of 2.25 cm). Spherical filter sand (Dansand A/S, Denmark) ranging between 0.4 and 0.8 mm (mean size 0.52 mm) was used as porous medium. The main component of the sand was silica (>99%) with a small fraction of Fe_2O_3 and CaO. The sand was acid-washed (1% hydrochloric acid) and rinsed repeatedly with DI. The zeta potential of the sand in tap water was -47.5 mV. The sand was wet packed in the column as uniformly as possible with constant tapping. The resulting porosity was approximately 0.41 corresponding to a total pore volume (PV) of 48.7±0.7 mL (based on fitting of the four tracer tests). Tap water was used to simulate groundwater, as Danish tap water consists of groundwater, which has undergone minimal treatments i.e. sand filtering and aeration. The tap water had a pH of 7.7 and an ionic strength of 12 mmol L^{-1}. The main ionic species were bicarbonate (310 mg L^{-1}), calcium (100 mg L^{-1}), chloride (85 mg L^{-1}), sulfate (45 mg L^{-1}), sodium (35 mg L^{-1}) and magnesium (15 mg L^{-1}). The water velocity was controlled by a peristaltic pump with a DG2 pump head (BT100-2J, Longer Precision Pump Co., Ltd, China) and introduced as a bottom-up flow. The sand column was equilibrated with the artificial groundwater (tap water) for at least 10 PV to obtain a uniform distribution of charges on the sand surfaces.

All the AuNP influent suspensions were prepared by mixing the stock suspension with a potassium bromide solution (solute tracer) and diluting with DI water to achieve a gold concentration of 40 mg L^{-1} and a bromide concentration of 6 mmol L^{-1}. The pH of all the AuNP influent suspensions was around 6 and no adjustment was made. The size distribution and zeta potential of the AuNPs in all the influent suspensions were characterized, and the changes in the size distribution over time (180 min) were measured to investigate the stability of the AuNPs (lack of aggregation) for the experimental period.

The steady state transport behavior was investigated by injection of 1 PV of AuNP influent suspension. The influent AuNP suspension was injected using the peristaltic pump at different flow rates (0.25, 0.5, 1 and 2 mL min^{-1}) with different corresponding interstitial velocities (0.14±0.02, 0.29±0.03,

0.59±0.06 and 1.22±0.12 cm min^{-1}), column residence times (209, 104, 51, 25 min) and Darcy velocities (0.06, 0.12, 0.24 and 0.50 cm min^{-1}), respectively. The flow velocities were selected to represent fast groundwater flow (0.06, 0.12 cm min^{-1}) and possible injection (0.24, 0.50 cm min^{-1}) scenarios. Moreover, the flow rates were feasible for column sampling and performance. Wall effects were assumed to be insignificant given a column-to-grain diameter ratio above 30 (Cohen and Metzner, 1981). After the NPs were introduced, artificial groundwater (tap water) continued to be introduced to the column. The effluents were collected at each 4 mL and analyzed for AuNPs by ultraviolet-visible (UV-Vis) spectrophotometry and bromide by ion chromatography (IC). The effluent samples from all three series with a Darcy velocity of 0.06 cm min^{-1} were analyzed by single particle inductively coupled plasma mass spectrometry (sp-ICP-MS) and full UV-Vis absorption spectra (400-700 nm) were recorded. The citrate AuNPs series at 0.06 cm min^{-1} (1.1-1.4 PV only) was selected to conduct DLS measurements for size distribution characterization.

1.4 Characterization and analytical methods

The AuNPs influent suspensions were characterized with regard to the size distribution (hydrodynamic diameter) and zeta potential by DLS measurements (triplicate at 25°C) using a Zetasizer Nano series (Malvern Instruments, USA). The zeta potential measurements of the porous media were conducted by rinsing the sand in tap water for 24 hours with constant stirring before testing the zeta potential of the supernatant. Cuvettes with 1 mL sample were used for size distribution, while disposable folded capillary zeta cells (DTS1060C) with an electric field were used for zeta potential measurements.

Sp-ICP-MS (NexION 350D, PerkinElmer, USA) was used to determine the size of the NP gold core (13-100 nm range). The influent samples of the three AuNPs suspension were characterized, and also the effluent samples at 0.06 cm min^{-1} to investigate the size variation of AuNPs during transport. All samples were diluted with Milli-Q water (18.2 MΩ) to concentrations below 0.1 µg L^{-1} to fall within the linear calibration range. The AuNPs were measured in single particle mode (time-resolved analysis). The dwell time was set to 1×10^{-4} s and the scan time to 100 s. Particle size and number concentration were calculated using spherical size as previously described (Pace et al., 2011). The spherical shape of the AuNPs was supported by Transmission Electron Microscopy (TEM) images (Tecnai T20 G^2 microscope at 200 kV) of all two of the three types of AuNPs (Appendix A, Fig. S1). The lower size limit of detection (13 nm) was calculated based on mean particle size for blank samples (Milli-Q water) with addition of three standard deviations.

The AuNP concentration in suspension was determined by UV-Vis spectrophotometry (UV-2600, Shimadzu, Japan). Calibration curves for the intensity of the absorbance maximum of the localized surface plasmon resonance (LSPR) of the AuNPs as a function of gold concentrations were linearly correlated (R^2>0.999). The full UV-Vis absorption spectra (400-700 nm) were also recorded for selected samples. The nonreactive soluble bromide tracer was measured by IC suppressed conductivity detection (ICS-5000, ThermoScientific, USA) as described by Mosthaf et al. (2018).

1.5 Data analysis

1.5.1 Colloidal filtration theory calculation

The transport of NPs is often described by colloidal filtration theory and Derjaguin-Landau-Verwey-Overbeek (DLVO) theory on colloidal stability assuming that the NPs (1-100 nm) act like a subclass of small diffusion dominated colloids and that the same basic transport principles apply to the NPs (Petosa et al., 2010). The DLVO theory is described in Appendix A. The transport and deposition of colloidal particles in saturated homogeneous porous media is described by the one-dimensional form of advection-dispersion equation coupled with deposition of particles onto collector surfaces (porous media grains) as expressed by (El Badawy et al., 2013; Rahman et al., 2013; Tufenkji and Elimelech, 2004):

$$\frac{\partial C}{\partial t} = D\frac{\partial^2 C}{\partial x^2} - v_x\frac{\partial C}{\partial x} - k_d C \qquad (1)$$

where C is the fluid-phase particle mass concentration (mg L^{-1}), D is the hydrodynamic dispersion coefficient (m^2 s^{-1}), x is distance along the column from the inlet (m), t is time (sec), v_x is the interstitial velocity (m sec^{-1}) and k_d (sec^{-1}) refers to the particle deposition rate coefficient, which is described as:

$$k_d = \frac{3(1-\theta)v}{2d_c\theta}\alpha\eta_0 \qquad (2)$$

where θ is the porosity of the porous media, v is the Darcy velocity (m sec^{-1}), d_c is the average grain size (m), α is the particle-collector attachment efficiency and η_0 is the single collector contact efficiency.

The deposition of NPs in porous media consists of two steps. First, the suspended NPs are transported to the vicinity of the sand surface; this process may be quantified by calculating η_0, which accounts for the hydrodynamics, particle size, density and Van der Waal forces. Second, the NPs attach to the sand surface after collision (Ben-Moshe et al., 2010), which is elucidated by calculating α. The removal efficiency of particles (η_r) can be presented as a function of η_0 and α:

$$\eta_r = -\frac{2}{3}\frac{d_c}{(1-\theta)L}\ln(C/C_0) = \alpha\eta_0 \qquad (3)$$

where C and C_0 are the particle concentrations (mg L^{-1}) of effluent and influent samples, and L is the length (m) of the packed column.

For η_0, the transport of NPs from the flowing groundwater to the vicinity of the collector is typically governed by three mechanisms: interception, gravitational sedimentation, and Brownian diffusion. Using the correlation equations described by Tufenkji and Elimelech (2004), the overall single collector contact efficiency can be calculated numerically by summing the contributions of each transport mechanism:

$$\eta_0 = \eta_D + \eta_I + \eta_G \qquad (4)$$

where η_D, η_I and η_G are the calculated dimensionless parameters for each of the transport mechanisms (Brownian diffusion, interception and gravitational sedimentation, respectively). The measured hydrodynamic diameter was used for the calculations. The attachment efficiency represents the fraction of the collisions between the suspended particles and collector grains that result in attachment. Under specific physicochemical conditions, data from column experiments can be used to determine the attachment efficiency (α) according to Eq. 3:

$$\alpha = -\frac{2}{3}\frac{d_c}{(1-\theta)L\eta_0}\ln(C/C_0) \qquad (5)$$

The maximum NP transport distance (L_T), defined as the distance where 99% of the injected NPs are deposited on the porous media, and the impact radius (L_R), defined as the distance where 50% of the injected NPs are suspended in the groundwater, can be predicted.

1.5.2 Analytical modelling

A simple analytical modelling approach has been used for data analysis. The concentration of suspended particles $C(x, t)$ at a column length x and time t was modeled by solution of the one-dimensional form of advection-dispersion equation coupled with deposition (eq. 1).

For a semi-infinite column initially free of particles, the 1D ADE can be solved for a step injection, where $C(0,t)$ is C_0 for the length of the injection (t_0) and zero at $t > t_0$, by use of Laplace transformation (van Genuchten, 1981):

$$C(x,t) = \begin{cases} C_0 H(x,t)\ for\ 0 < t \le t_0 \\ C_0\big(H(x,t) - H(x,t-t_0)\big)\ for\ t > t_0 \end{cases} \qquad (6)$$

where $H(x, t)$ is given by:

$$H(x,t) = \frac{1}{2}exp\left(\frac{(v_x-u)x}{2D}\right)erfc\left(\frac{Rx-ut}{2\sqrt{DRt}}\right) + \frac{1}{2}exp\left(\frac{(v_x+u)x}{2D}\right)erfc\left(\frac{Rx+ut}{2\sqrt{DRt}}\right) \qquad (7)$$

where R is the retardation factor and u is given by:

$$u = v_x\sqrt{1+\frac{4k_dD}{{v_x}^2}} \qquad (8)$$

Values for D, k_d and v_x can be determined simultaneously from the direct fit of the observed particle breakthrough curves.

2 Results and discussion

2.1 Characterization of gold nanoparticles

Characteristics related to the three types of AuNPs influent suspensions and the citrate AuNP stock suspension are listed in **Table 1**. Results showed that all the AuNPs in the influent were slightly charged with a zeta potential around -12 mV resulting in repulsive interactions between the media and the AuNPs. The sp-ICP-MS measurements give the diameter of the gold core, while the larger hydrodynamic diameter of AuNPs coated by PVA-COOH indicates the thickness of the adsorbed polymer layer. For the polymer coated AuNPs, the hydrodynamic radius is 9 and 12 nm larger than the core radius for the 1:0.5 and 1:10 particle/polymer ratio, respectively. For citrate AuNPs, where no polymer brush layer exists, the two measurements are comparable. The measurements have been used for DLVO calculations (cf. Appendix A).

The mixing of the stock suspensions with tracer solution (6 mmol L^{-1}) did not affect the stability of the mainly sterically stabilized PVA-COOH AuNPs (within 180 min), but initially resulted in larger less stable citrate AuNPs (**Table 1**) with no additional major destabilization (within 180 min). Since citrate AuNPs are purely electrostatically stabilized the observed impact of the increased ionic strength was expected. Since the tracer mixed influent AuNP suspension remained stable (**Fig. S2**) for the duration of the experiment (180 min), aggregation of AuNPs in the column would mainly be due to the interaction of NPs with the porous media and/or the artificial groundwater (tap water).

Table 1 Parameters for three types of AuNPs in the column influent suspension (ionic strength 6 mmol L^{-1}) and the citrate AuNPs stock suspension before mixing with KBr solution

Type of AuNPs	pH	Hydrodynamic diameter (DLS) (nm)	Core diameter (sp-ICP-MS) (nm)	Zeta potential (mV)
AuNPs:Citrate (stock)	5.48	22.0±2.7	23.0±3.9	-38
AuNPs:Citrate (influent)	5.87±0.04	27.3±1.3	29.0±6.6	-12.2±0.4
AuNPs:PVA-COOH (1:0.5)	6.25±0.08	35.2±4.9	18.0±2.5	-11.5±2.2
AuNPs:PVA-COOH (1:10)	6.09±0.10	43.7±0.7	19.7±2.3	-12.3±1.0

2.2 AuNP transport in porous media columns

The breakthrough curves (BTCs) illustrate the transport of tracer (**Fig. 1a**) and AuNPs (**Fig. 1b-d**) in the column. The parameters fitted with the 1D ADE are given in **Table S1**.

The tracer experiments were used to fit the interstitial velocity and the dispersion coefficients at each flow velocity using the 1D ADE, which could successfully simulate the BTC (R^2 0.999±0.001). The tracer showed close to complete recovery (cf. **Fig. 2**).

The type of stabilization and the polymer surface coverage of the AuNPs significantly impact the transport of AuNPs in porous media. AuNPs:PVA-COOH (1:10) were very mobile in the porous media without significant retention (**Fig. 2**) and no retardation (**Fig. 1b**), and hence exhibiting a similar behavior as the bromide tracer. The BTCs at all four velocities were almost identical and could be successfully simulate by the 1D ADE (R^2 0.994±0.004). The best fit for the two lowest velocities was achieved with a low particle deposition rate coefficient of around 1×10^{-4} min^{-1}, while the two highest velocities were best fitted without any deposition.

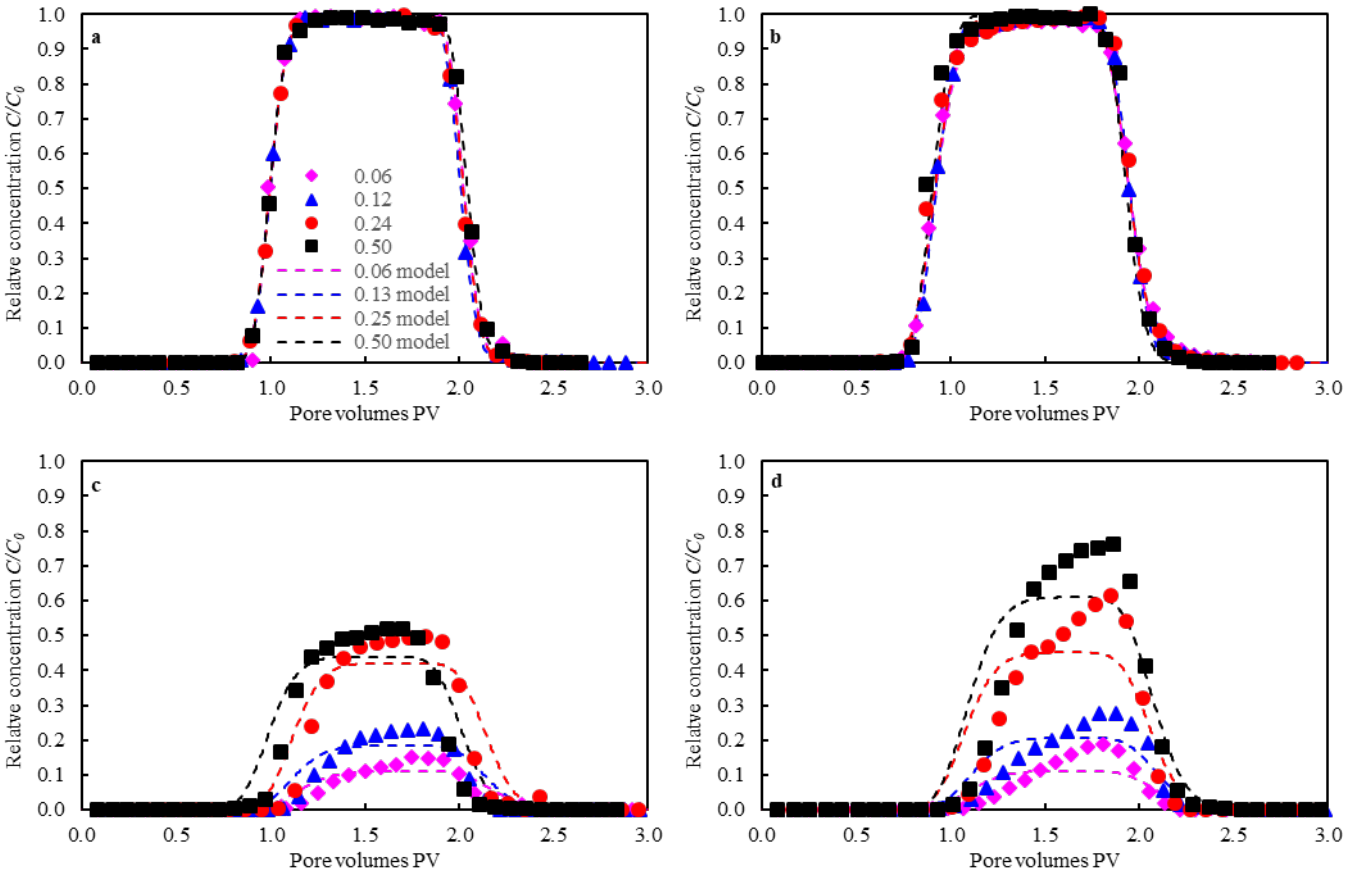

Fig.1 Breakthrough curve data (points) and best fit to the 1D ADE equation (lines) for the four Darcy velocities: (a) Bromide tracer, (b) AuNP.s:PVA-COOH (1:10), (c) AuNPs:PVA-COOH (1:0.5), and (d) citrate AuNPs

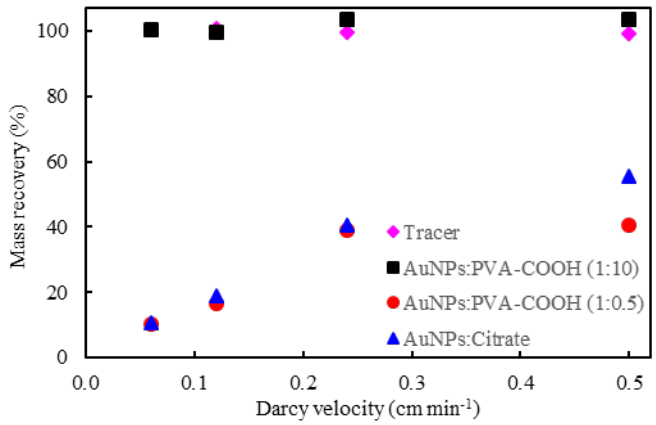

Fig.2 The mass recovery of the bromide tracer and the three types of AuNPs in the column effluent at the four Darcy velocities.

The decrease in polymer surface coverage with a lower particle/polymer ratio (1:0.5) had a significant impact on the transport of the AuNPs. The fit with the 1D ADE was poorer (R^2 0.90±0.02) and slightly more so at lower flow velocities. The poorer fit is seen primarily as a result of a slight rising trend of the plateau area indicating that processes not accounted for by the simple deposition term in the 1D ADE are occurring. The rising trend is generally an indication of deposition sites becoming unavailable (blocking) as the AuNPs passes though the column. The deposition sites may be blocked by already deposited NPs, where the deposited particles have been found to form a shadow zone with less downgradient depostition. This is further promoted by enlarged particle sizes from aggregation and higher flow velocities (Ko and Elimelech, 2000; Rahman et al., 2013). Alternatively, excess of the stabilizing agent has been found to block the attachment sites by adsorbing to them (Becker et al., 2015). However, only a minimal excess of polymer in solution is expected at this particle/polymer ratio (1:0.5). At a ratio with more excess polymer in solution, the impact on transport from adsorption site blocking by adsorbed polymer is likely, and for the 1:10 particle/polymer ratio it cannot be ruled out that excess polymer contributes to the very high mobility. Larger particle deposition rate coefficients of 1.0×10^{-2} to 3.4×10^{-2} min^{-1} were found (increasing with velocity), which resulted in lower mass recovery (**Fig. 2**).

The type of stabilization also had a significant impact on the transport of the AuNPs. The purely electrostatically stabilized (citrate) AuNPs also showed poorer recovery (**Fig. 2**), which was very similar to that of AuNPs:PVA-COOH (1:0.5) (except at 0.5 cm min^{-1}). The fit with the 1D ADE was the poorest (R^2 0.86±0.05) as the pronounced rising trend of the BTC plateau (**Fig. 1d**) could not be fitted, and a delay in the breakthrough was observed. Compared to PVA-COOH (1:0.5) AuNPs, the blocking appears much more distinct. The rising trend is much steeper, and the recovery keeps

increasing with the flow velocity (increased shadow zone). The excess of citrate (anionic) is not expected to block attachment sites on the negatively charged sand media (Mazurenka et al., 2008), whereby the blocking is most likely a pure result of deposition of the less stable particles (**Fig. S3b**) and aggregates. The particle deposition rate coefficients resembled the AuNPs:PVA-COOH (1:0.5) with values of 0.9×10^{-2} to 1.8×10^{-2} min^{-1}.

In general, considering the mass recovery and maximum effluent concentration C/C_0, the mobility of the three types of AuNPs followed the order of AuNPs:PVA-COOH (1:10) >> citrate AuNPs ≥ AuNPs:PVA-COOH (1:0.5). The similarities in the transport of AuNPs:PVA-COOH (1:0.5) and citrate AuNPs are surprising. The electrostatic stability of the AuNPs are similar (**Fig. S3a**, **Table 1**), but the additional steric stabilization of AuNPs:PVA-COOH (1:0.5) was expected to enhance the mobility significantly (**Fig. S3b**), like it is seen for AuNPs:PVA-COOH (1:10). A closer look at the governing mechanisms behind the transport behavior is needed.

2.3 Colloidal filtration theory

Colloid filtration theory is applied to interpret the BTCs of the AuNPs. The calculated single collector efficiency (eq. 4; **Table S2**) confirmed that diffusion was the predominant contribution (>99%) of the total collector efficiency as expected for NPs smaller than 100 nm (Rahman et al., 2013). Due to the small size of all the AuNPs, the contribution of interception and gravitation was negligible.

The values of the single collector efficiency (η_0) of AuNPs increased in the order AuNPs:PVA-COOH 1:10 < AuNPs:PVA-COOH (1:0.5) < citrate AuNP at all velocities (**Fig. 3a**).

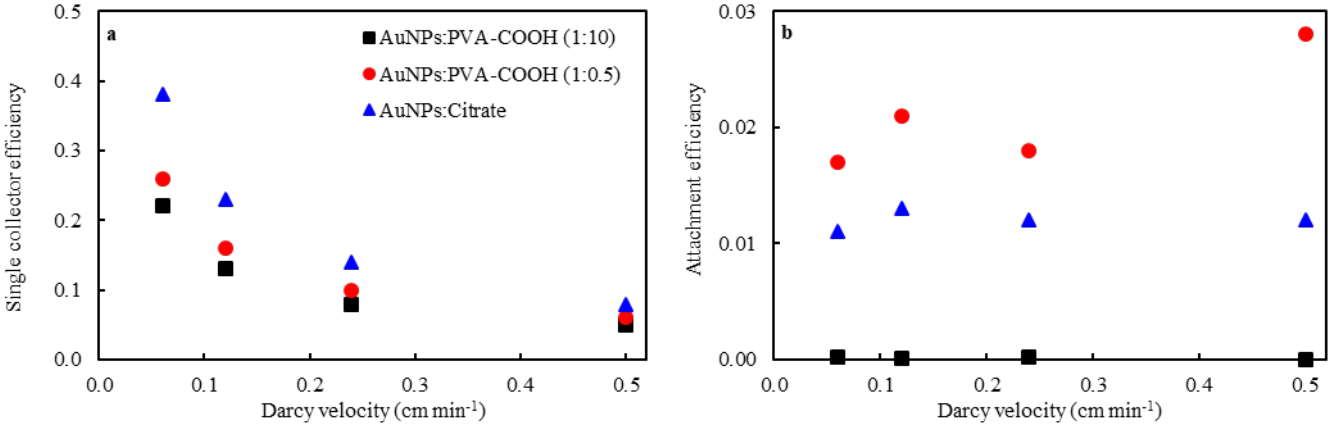

Fig. 3 The effect of the Darcy velocity on the (a) single collector efficiency η_0 (sum of η_D, η_I, and η_G), and (b) the attachment efficiency, α, for the three types of AuNPs.

The single collector efficiency is thereby negatively correlated with the particle size; the smaller particles have higher η_0, and thus the highest mass transfer from the bulk solution toward the aquifer material surface by Brownian diffusion. It should also be noted, that the single collector efficiency becomes smaller with increasing water velocity, which is consistent with the expectations (e.g. He et al., 2009). Generally, the Darcy velocity affects the removal efficiency by governing the frequency of NPs transport from the flowing (ground)water to the vicinity of the collector (η_0).

The attachment efficiency (α) varies as a function of factors such as ionic strength, pH, the solution chemistry, the properties of the NPs and the characteristics of the collector surface (Wang et al., 2016). The attachment efficiencies calculated (eq. 3) based on the BTCs were very similar at various Darcy velocities (**Table S2** and **Fig. 3b**) for each of the AuNP types and increased in the order AuNPs:PVA-COOH 1:10 << citrate AuNP < AuNPs:PVA-COOH (1:0.5) at all velocities. Elimelech (1992) also reported that α is unaffected by flow velocities, whereas Kim and Lee (2014) observed an increase with increasing water velocities until a critical value where no further increase was observed. In our experiment, such a critical value is not observed and α is independent of water velocity in the experimental range. The drastically lower attachment efficiency of AuNPs:PVA-COOH (1:10) compared to the two other types of AuNPs indicates that the strong steric repulsion provided by the high concentration of PVA-COOH (**Fig. S3b**) can be responsible for the lower attachment efficiency and thus minimal deposition.

The predicted impact radius ($C/C_0 = 0.5$) from a point of release in groundwater with comparable conditions (such as grain diameter and porosity) to the column experiment can be estimated (eq. 5) from the determined filtration parameters (cf. **Fig. S6**). For the lower Darcy velocities, typical for groundwater (0.06-0.12 cm min^{-1}), this resulted in predicted impact radius on the centimeter scale (20-30 cm) for the citrate AuNPs and AuNPs:PVA-COOH (1:0.5), while it for the AuNPs:PVA-COOH (1:10) increased to several meters (20-40 m). The parameters from the colloidal filtration theory thereby confirm the observed similarities in the transport of citrate AuNPs and AuNPs:PVA-COOH (1:0.5) and the superior transport properties of the AuNPs:PVA-COOH (1:10). The risk of spreading of the NPs in the subsurface environment is thereby low for the electrostatically stabilized NPs and the weakly steric stabilized NPs, while the strongly steric stabilized NPs are very mobile in the subsurface and could potentially reach downgradient receptors.

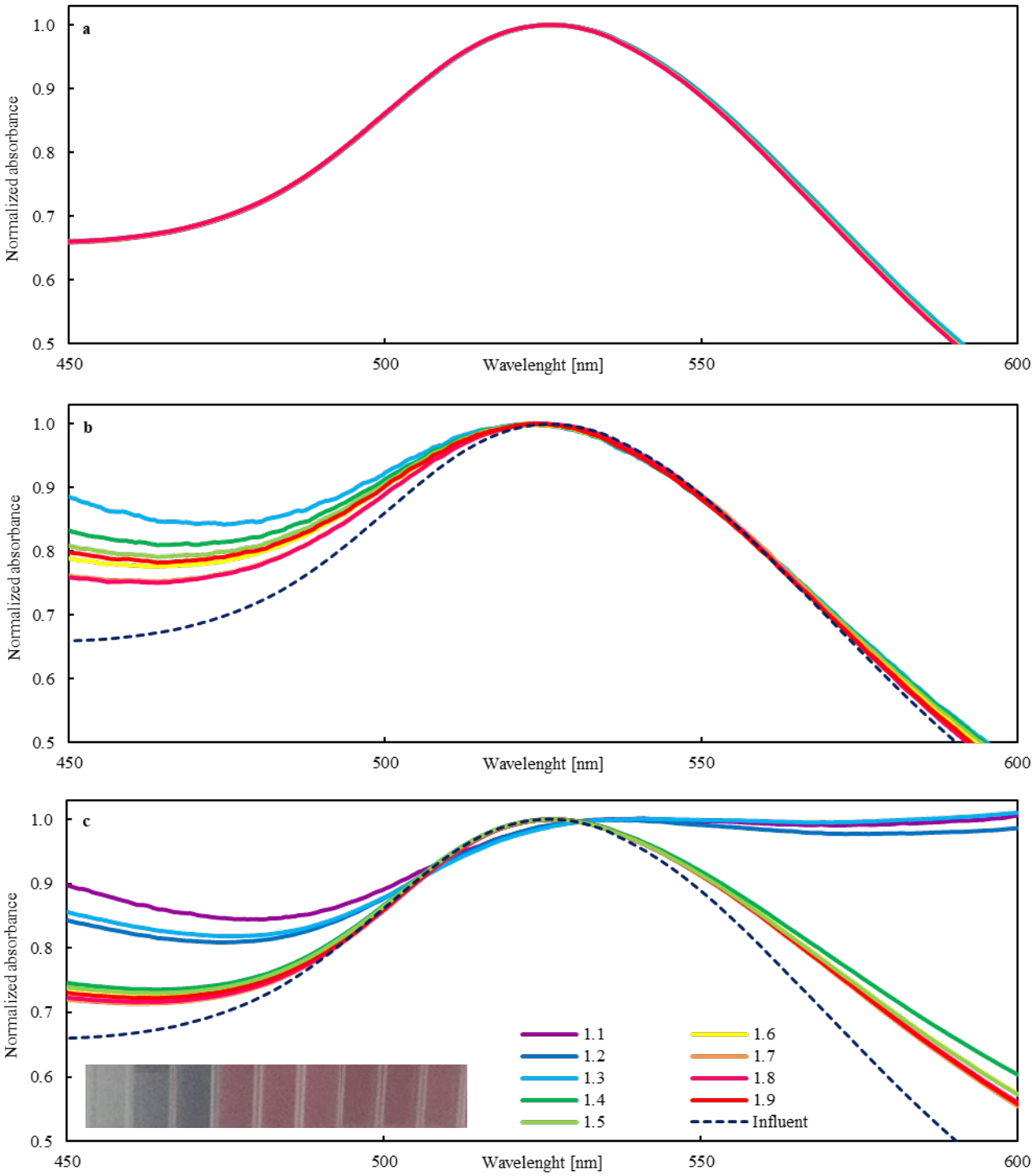

Fig.4 UV-Vis spectra for the column influent and effluents (1.1-1.9 PV) at a Darcy velocity of 0.06 cm min^{-1} for the three types of AuNPs stabilized by: (a) PVA-COOH (1:10) at 1.1-1.8 PV, (b) PVA-COOH (1:0.5) at 1.3-1.9 PV and (c) citrate at 1.1-1.9 PV. The UV-Vis spectra are given for effluent PVs (legends) representing the BTC plateau area (cf. **Fig. 1**); specifically for citrate AuNPs the visually observable red shift (1.1-1.3 PV) is also seen on the picture of the effluent color change (1.1-1.9 PV).

2.4 Particles transformation during transport

It was observed that the citrate AuNPs effluent suspension changed color from red to dark blue at the front of the plume (1.1-1.3 PV) at all velocities (**Fig. 4c**) as the electrostatically stabilized citrate AuNPs are sensitive to ionic changes at the mixing front (**Fig. S4a**); no visually observable color change was observed for any of the PVA-COOH coated AuNPs or for the later part of the citrate AuNP breakthrough. Effluent samples from the plateau area of the BTCs (Darcy velocity of 0.06 cm min^{-1}) were investigated for the gold core size (sp-ICP-MS) and the UV-Vis absorbance spectra (**Fig. 4**). Also, for the citrate AuNPs selected effluent samples (PV 1.1-1.4) were investigated for the hydrodynamic diameter (DLS) to determine the size of the effluent aggregates, which were outside of the sp-ICP-MS size range (>100 nm). The hydrodynamic diameter was not measured for any other effluent samples as no indications of larger particles were seen.

The results revealed that no significant change occurred for the AuNPs with PVA-COOH (1:10) coating (**Fig. 4a**) in the porous media. The particles in the effluent were stable and appeared identical to the influent suspension throughout the effluent pulse. This was confirmed by sp-ICP-MS measurements that showed AuNP core sizes of 18.5±1.9 nm for the whole pulse, which is comparable to the 19.7 nm in the influent suspension (**Table 1**). The overall stability and mobility of the PVA-COOH (1:10) stabilized AuNPs is very high.

For PVA-COOH (1:0.5) stabilized AuNPs (**Fig. 4b**) a lower stability is observed than for PVA-COOH (1:10) stabilized AuNPs. This is observed as a spectral shift in the effluent compared to the influent suspension. A minor blue shift can be seen compared to the maximum absorbance peak for the influent suspension (527.5 nm). The shift is larger for the front of the pulse (around 5 nm) than in the center/tail of the pulse (around 2.5 nm). The blue shift can result from smaller AuNPs particles in the front of the pulse. The sp-ICP-MS measurements showed AuNP core sizes of 19.5±1.3 nm for the whole pulse, which is slightly larger but similar to the stock suspension (18.0 nm). The blue shift in the effluent is thereby not be related to smaller AuNP core sizes, but more likely to the polymer layer. The shift in the maximum absorption wavelength can be used to estimate the polymer layer thickness, due to the impact of the polymer on the local dielectric environment (D'Agata et al., 2017). A blue shift can thereby be linked with a somewhat thinner polymer brush layer on the AuNPs in the effluent; the expected peak for a polymer free 19 nm AuNPs would be around 518 nm (Fjordbøge et al., 2019). In the porous media the polymer may be lost through ligand exchange with the sand, which would significantly impact the stability. The particles are not expected to be stable in the porous media at a polymer layer thickness below 3 nm (**Fig. S4b**). A loss of the steric stabilization could

explain the lower than expected mobility of PVA-COOH (1:0.5) stabilized AuNPs. The electrostatic stability of the PVA-COOH (1:0.5) stabilized AuNPs is similar to that of citrate AuNPs (**Fig. S3a**), which show more comparable transport.

For citrate stabilized AuNPs (**Fig. 4c**, cf. **Fig. S7** for full spectra) a significant destabilization occurs in the front of the pulse (1.1-1.3 PV), where the hydrodynamic diameter increased from 27 nm to the range of 600-1400 nm. These aggregates are expected to be relatively mobile based on very low single collector efficiencies (**Fig. S5**). The destabilization in the front of the pulse may explain the delayed breakthrough around 1.2 PV (**Fig. 1d**) as both the deposited particles and these larger mobile gold aggregates in the effluent would not be detected by the UV-Vis measurements at the wavelength used for the quantification of the AuNPs. The red-shift and the enlarged particles in the effluent indicate that aggregation of the AuNPs was induced in the porous media, which is attributed to the higher ionic strength imparted by mixing with the artificial groundwater (tap water) at the front of the AuNP plume. The citrate AuNPs are barely stable in the influent suspension (energy barrier <1.5kT) and at the higher ionic strength of the tap water (12 mmol L^{-1}) only a slight increase in the zeta potential (from -12 to -10 mV) would result in the energy profile turning negative (**Fig. S4a**). It has also previously been reported, that citrate AuNPs were immobilized in Danish tap water (12 mmol L^{-1}) and sand when using a pulse injection of 0.2 PV at a 0.25 cm min^{-1} Darcy velocity (Fjordbøge et al., 2019). The size of the injected pulse (mass of AuNPs) would thereby seem of importance for the transport. As earlier described (**Fig. 1d**), blocking facilitated by aggregation and higher flow velocities occurred as the citrate AuNPs were transported in the saturated porous media. The blocking phenomenon can also contribute to the explanation of immobilization of a small volume pulse injection (Fjordbøge et al., 2019) compared to the larger pulse injected in these experiments, as the amount would be insufficient to fill up sufficient attachment sites on the grain surface to induce significant blocking.

The findings revealed that the PVA-COOH coating provide stability of NPs if the surface coverage is sufficient after ligand exchange with the media. Overall, a combination of mechanisms including extended DLVO forces (such as steric force), filtration theory, ligand exchange and blocking was involved. Consideration of these factors is important for interpretation and prediction for the fate and transport of ENPs in the subsurface.

3 Conclusions

It was found that both the properties of the stabilizer (type and coverage) and the Darcy velocity are key factors for AuNP transport in porous media. For the NPs with strong steric stabilization, the mobility was independent of the water velocity and resembled that of the solute tracer (Br) with full recovery and no retardation. However, for the purely electrostatically stabilized NPs and the weakly sterically stabilized NPs, the transport was dependent on the water velocity and significantly reduced compared to the solute tracer. The recovery of NPs in the porous media column increased with increasing water velocity (decreasing residence time and single collector efficiency, η_0). For the electrostatically stabilized NPs, aggregation was induced during transport in porous media and large aggregates (600-1400 nm) were transported in the front of the plume (low η_0). The aggregation is likely a result of mixing with tap water of higher ionic strength (12 mmol L^{-1}), which DLVO calculations indicate would destabilize the particles. The transport of the electrostatically stabilized AuNPs in this study, was facilitated by the blocking mechanism, as seen by the pronounced rising plateau of the column breakthrough curves, which can be enhanced by the shadow zone effect of deposited aggregates and higher flow rates. The weakly sterically stabilized NPs were found to lose stability during transport as well as a reduction in size (blue shift). Since no change in the gold core size was observed (sp-ICP-MS), the reduced size is likely linked with a reduced thickness of the polymer brush on the surface. DLVO calculations indicate that loss of stability is a likely result of polymer being lost through ligand exchange with the porous media. At a polymer layer thickness below 3 nm, the particles are not expected to have sufficient steric forces to overcome the attraction energy resulting in particle deposition. This could also have implication for the stronger sterically stabilized NPs at longer transport distances (more interaction with the porous media) and should be investigated further.

It is concluded that the water velocity will have a negligible impact on the NP transport and deposition when attachment is highly unfavorable (α in the range of 10^{-7}-10^{-4}) as seen for the AuNPs with strong steric stabilization, whereas it has a significant impact when deposition occurs. To obtain highly unfavorable attachment conditions, sufficient polymer coating is needed to achieve strong steric repulsion, which will then be the main force contributing to the transport of NPs in the porous media. This highlights the importance of sufficient surface coating to achieve enhanced mobility, but also the increased risk of spreading to down-gradient receptors. While high velocity injections will be needed to obtain an impacted area of just a few meters if attachment occurs, the NPs with strong steric stabilization can potentially be transported hundreds of meters. Further research is still needed to take

the subsurface heterogeneity, the concentration of NPs and dynamic changes of NPs into consideration.

Acknowledgments

The presented work was funded by the joint Korea Advanced Institute of Science & Technology and Technical University of Denmark (KAIST-DTU) signature project, INtegrated WAter Technology, also Chunyu Wen's stay at the Technical University of Denmark was funded by the China Scholarship Council.

Appendix A. Supplementary data

Supplementary data associated with this article can be found in the online version.

References

Bayat, A.E., Junin, R., Derahman, M.N., Samad, A.A., 2015. TiO_2 nanoparticle transport and retention through saturated limestone porous media under various ionic strength conditions. Chemosphere 134, 7–15.

Becker, M.D., Wang, Y., Pennell, K.D., Abriola, L.M., 2015. A multi-constituent site blocking model for nanoparticle and stabilizing agent transport in porous media. Environ. Sci.: Nano, 2, 155-166.

Ben-Moshe, T., Dror, I., Berkowitz, B., 2010. Transport of Metal Oxide Nanoparticles in Saturated Porous Media. Chemosphere 81(3), 387–393.

Chan, M.Y., Vikesland, P.J., 2014. Porous Media-Induced Aggregation of Protein-Stabilized Gold Nanoparticles. Environ. Sci. Technol. 48(3), 1532–40.

Cirtiu, C.M., Raychoudhury, T., Ghoshal, S., Moores, A., 2011. Systematic comparison of the size, surface characteristics and colloidal stability of zero valent iron nanoparticles pre- and post-grafted with common polymers. Colloid. Surface. A, 390, 95–104.

Cohen, Y., Metzner, A.B., 1981. Wall Effects in Laminar Flow of Fluids through Packed Beds. AlChE J. 27(5), 705–715

D'Agata, R., Palladino, P., Spoto, G., 2017. Streptavidin-coated gold nanoparticles: critical role of oligonucleotides on stability and fractal aggregation. Beilstein J. Nanotechnol. 8, 1–11.

Daniel, M.C., Astruc, D., 2004. Gold Nanoparticles: Assembly, Supramolecular Chemistry, Quantum-Size-Related Properties, and Applications toward Biology, Catalysis, and Nanotechnology. Chem. Rev. 104(1), 293–346.

Dong, J., Ding, L., Wen, C., Hong, M., Zhao, Y., 2013. Effects of Geochemical Constituents on the Zero-Valent Iron Reductive Removal of Nitrobenzene in Groundwater. Water Environ. J. 27(1), 20–28.

El Badawy, A.M, Hassan, A.A., Scheckel, K.G., Suidan, M.T., Tolaymat, T.M., 2013. Key Factors Controlling the Transport of Silver Nanoparticles in Porous Media. Environ. Sci. Technol. 47(9), 4039–4045.

Elimelech, M., 1992. Predicting Collision Efficiencies of Colloidal Particles in Porous Media. Water Res. 26(1), 1–8.

Fjordbøge, A.S., Uthuppu, B., Jakobsen, M.H., Fischer, S.V., Broholm, M.M., 2019. Mobility of electrostatically and sterically stabilized gold nanoparticles (AuNPs) in saturated porous media. Environ. Sci. Pollut. R. 26, 29460–29472.

van Genuchten, M.T., 1981. Analytical Solutions of the One-Dimensional Convective-Dispersive Solute Transport Equation. U.S. Department of Agriculture, Technical Bulletin No. 1661, 151 p.

Godinez, I.G., Darnault, C.J.G., 2011. Aggregation and Transport of Nano-TiO2 in Saturated Porous Media: Effects of pH, Surfactants and Flow Velocity. Water Res. 45(2), 839–851.

Grieger, K.D., Fjordbøge, A., Hartmann, N.B., Eriksson, E., Bjerg, P.L., Baun, A., 2010. Environmental Benefits and Risks of Zero-Valent Iron Nanoparticles (nZVI) for in Situ Remediation: Risk Mitigation or Trade-Off? J. Contam. Hydrol. 118(3–4), 165–183.

He, F., Zhang, M., Qian, T., Zhao, D., 2009. Transport of Carboxymethyl Cellulose Stabilized Iron Nanoparticles in Porous Media: Column Experiments and Modeling. J. Colloid. Interf. Sci. 334(1), 96–102.

Hotze, E.M, Phenrat, T., Lowry, G.V., 2010. Nanoparticle Aggregation: Challenges to Understanding Transport and Reactivity in the Environment. J. Environ. Qual. 39, 1909–1924.

Kim, C., Lee, S., 2014. Effect of Seepage Velocity on the Attachment Efficiency of TiO_2 Nanoparticles in Porous Media. J. Hazard. Mater. 279, 163–168.

Ko, C.H., Elimelech, M., 2000. The “Shadow Effect” in Colloid Transport and Deposition Dynamics in Granular Porous Media: Measurements and Mechanisms. Environ. Sci. Technol. 34, 3681–3689.

Li, C., Li, D.,Wan, G., Xu, J., Hou, W., 2011. Facile synthesis of concentrated gold nanoparticles with low size-distribution in water: temperature and pH controls. Nanoscale Res. Lett. 6, 440

Liu, J., Liu, A., Zhang, W.X., 2016. The Influence of Polyelectrolyte Modification on Nanoscale Zero-Valent Iron (nZVI): Aggregation, Sedimentation, and Reactivity with Ni(II) in Water. Chem. Eng. J. 303, 268–274.

Louie, S.M., Tilton, R.D., Lowry, G.V., 2016. Critical Review: Impacts of Macromolecular Coatings on Critical Physicochemical Processes Controlling Environmental Fate of Nanomaterials. Environ. Sci.: Nano 3(2), 283–310.

Mazurenka, M., Hamilton, S.M., Unwin, P.R., Mackenzie, S.R., 2008. In-Situ Measurement of Colloidal Gold Adsorption on Functionalized Silica Surfaces. J. Phys. Chem. C 112(16), 6462–6468.

Montaño, M.D., Lowry, G.V., von der Kammer, F., Blue, J., Ranville, J.F., 2014. Current status and future direction for examining engineered nanoparticles in natural systems. Environ. Chem. 11, 351–366.

Mosthaf, K., Brauns, B., Fjordbøge, A.S., Rohde, M.M., Kerrn-Jespersen, H., Bjerg, P.L., et al., 2018. Conceptualization of flow and transport in a limestone aquifer by multiple dedicated hydraulic and tracer tests. J. Hydrol. 561, 532–546.

O'Carroll, D., Sleep, B., Krol, M., Boparai, H., Kocur, C., 2013. Nanoscale Zero Valent Iron and Bimetallic Particles for Contaminated Site Remediation. Adv. Water Resour. 51, 104–122.

Pace, H.E., Rogers, N.J., Jarolimek, C., Coleman, V.A., Higgins, C.P., Ranville, J.F., 2011. Determining Transport Efficiency for the Purpose of Counting and Sizing Nanoparticles via Single Particle Inductively Coupled Plasma Mass Spectrometry. Anal. Chem. 83(24), 9361–69.

Panyala, N.R., Peña-Méndez, E.M., Havel, J. 2009., Gold and nano-gold in medicine: overview, toxicology and perspectives. J. Appl. Biomed. 7, 75–91.

Petosa, A.R., Jaisi, D.P., Quevedo, I.R., Elimelech, M., Tufenkji, N., 2010. Aggregation and Deposition of Engineered Nanomaterials in Aquatic Environments: Role of Physicochemical Interactions. Environ. Sci. Technol. 44, 6532–6549.

Phenrat, T., Saleh, N., Sirk, K., Kim, H.J., Tilton, R.D., Lowry, G.V., 2008. Stabilization of Aqueous Nanoscale Zerovalent Iron Dispersions by Anionic Polyelectrolytes: Adsorbed Anionic Polyelectrolyte Layer Properties and Their Effect on Aggregation and Sedimentation. J. Nanopart. Res. 10(5), 795–814.

Rahman, T., George, J., Shipley, H.J., 2013. Transport of Aluminum Oxide Nanoparticles in Saturated Sand: Effects of Ionic Strength, Flow Rate, and Nanoparticle Concentration. Sci. Total Environ. 463–464, 565–571.

Saleh, N., Sirk, K., Liu, Y., Phenrat, T., Dufour, B., Matyjaszewski, K., et al., 2007. Surface Modifications Enhance Nanoiron Transport and NAPL Targeting in Saturated Porous Media. Environ. Eng. Sci. 24(1), 45–57.

Sangani, M.F., Owens, G., Fotovat, A., 2019. Transport of engineered nanoparticles in soils and aquifers. Environ. Rev. 27, 43–70.

Tian, Y., Gao, B., Wu, L., Muñoz-Carpena, R., Huang, Q., 2012. Effect of Solution Chemistry on Multi-Walled Carbon Nanotube Deposition and Mobilization in Clean Porous Media. J. Hazard. Mater. 231–232, 79–87.

Toloni, I., Lehmann, F., Ackerer, P., 2014. Modeling the Effects of Water Velocity on TiO_2 Nanoparticles Transport in Saturated Porous Media. J. Contam. Hydrol. 171, 42–48.

Tufenkji, N., Elimelech, M., 2004. Correlation Equation for Predicting Single-Collector Efficiency in Physicochemical Filtration in Saturated Porous Media. Environ. Sci. Technol. 38(2), 529–536.

Wang, M., Gao, B., Tang, D., 2016. Review of Key Factors Controlling Engineered Nanoparticle Transport in Porous Media. J. Hazard. Mater. 318, 233–246.

Wang, D., Su, C., Liu, C., Zhou, D., 2014. Transport of Fluorescently Labeled Hydroxyapatite Nanoparticles in Saturated Granular Media at Environmentally Relevant Concentrations of Surfactants. Colloid. Surface. A 457(1), 58–66.

Yang, X., Zhang, Y., Chen, F., Yang, Y., 2015. Interplay of Natural Organic Matter with Flow Rate and Particle Size on Colloid Transport: Experimentation, Visualization, and Modeling. Environ. Sci. Technol. 49(22), 13385–13393.

Zhao, X., Liu, W., Cai, Z., Han, B., Qian, T., Zhao, D., 2016. An Overview of Preparation and Applications of Stabilized Zero-Valent Iron Nanoparticles for Soil and Groundwater Remediation. Water Res. 100, 245–266.